Onset of chaotic symbolic synchronization between population inversions in an array of weakly coupled Bose-Einstein condensates

C. L. Pando L.
IFUAP, Universidad Autónoma de Puebla, Apdo. Postal J-48, Puebla, Pue. 72570, Mexico

E. J. Doedel
Concordia University, 1455 Boulevard de Maisonneuve West, Montreal, Quebec, Canada H3G 1M8
(Received 20 July 2004; revised manuscript received 13 December 2004; published 3 May 2005)

We investigate the onset of chaotic dynamics of the one-dimensional discrete nonlinear Schrödinger equation with periodic boundary conditions in the presence of a single on-site defect. This model describes a ring of weakly coupled Bose-Einstein condensates with attractive interactions. We focus on the transition to global stochasticity in three different scenarios as the defect is changed. We make use of a suitable Poincaré section and study different families of stationary solutions, where certain bifurcations lead to global stochasticity. The global stochasticity is characterized by chaotic symbolic synchronization between the population inversions of certain pairs of condensates. We have seen that the Poincaré cycles are useful to gain insight in the dynamics of this Hamiltonian system. Indeed, the return maps of the Poincaré cycles have been used succesfully to follow the orbit along the stochastic layers of different resonances in the chaotic self-trapping regime. Moreover, the time series of the Poincaré cycles suggests that in the global stochasticity regime the dynamics is, to some extent, Markovian, in spite of the fact that the condensates are phase locked with almost the same phase. This phase locking induces a peculiar local interference of the matter waves of the condensates.

DOI: 10.1103/PhysRevE.71.056201 PACS number(s): 05.45.−a, 42.65.Tg, 87.10.+e, 42.25.Bs

I. INTRODUCTION

A large number of recent investigations have been devoted to studying the combined effects of disorder and nonlinearity in one-dimensional lattices. A typical theoretical model within this category is the discrete nonlinear Schrödinger equation (DNLSE) [1]. This equation describes a large class of discrete nonlinear systems such as optical fibers [2,3], polarons [4], small molecules such as benzene [4,5], and, more recently, dilute Bose-Einstein condensates trapped in a multiwell periodic potential [6]. One of the main effects in these lattices is localized excitations in perfectly periodic but strongly nonlinear systems [1,7,8]. We refer to discrete breathers, also known as intrinsic localized modes [1]. These are spatially localized, time-periodic, and stable stationary solutions of the DNLSE [1], and have been observed in many physical systems [8]. Experimentalists are currently interested in considering breathers in Bose-Einstein condensates [8].

The experimental observation of Bose-Einstein condensation (BEC) in a dilute gas of trapped atoms in an optical multiwell lattice, created by a far-detuned, standing-wave laser beam [9], has generated much interest in the dynamical properties of this state of matter. The condensates can coherently tunnel between interwell barriers. The heights of the barriers can be adjusted since they are proportional to the intensity of the laser beam. These experimental techniques have allowed direct observation of several phenomena originally believed to belong to solid-state physics such as quantum phase transitions [10] and Josephson regimes [9,11]. The evolution of this BEC is governed by the Gross-Pitaevskii equation and can be mapped, in the tight binding approximation, to a DNLSE [6]. Here, we consider the nonlinear dynamics of the DNLSE in a ring geometry in the presence of a single defect. In a BEC the defects can be created with additional lasers or magnetic fields. A double-well trapping potential was obtained by superimposing a sharp barrier induced by optical and magnetic traps [12]. In this way, two BECs were produced, one on each side of the barrier [12]. A theoretical model describing two interacting BECs considered this experiment [13]. Indeed, the possibility to carry out experiments with a small number of condensates in a ring geometry will become a reality, as soon as greater control of the microtrap technology is achieved [14].

The DNLSE is a vast subject with many different and relevant issues such as the dynamics of discrete breathers in one- or two-dimensional infinite lattices [1], propagation of excitations in the presence of disorder [15], and mobility and interaction of breathers [7]. Motivated by the dynamics of BEC, we concentrate on the special issue concerning the onset of chaos in the DNLSE with a small number of oscillators. The DNLSE is a nonlinear Hamiltonian system with M degrees of freedom, where M refers to the number of condensates. The DNLSE, as is well known, has two constants of motion [1]. Therefore, when $M=2$, the DNLSE is integrable. However, when $M\geqslant 3$, the DNLSE can exhibit an amazing degree of complexity. The chaotic dynamics for $M=3$ and 4 was studied, to our knowledge, for the first time almost two decades ago [16], considering, in particular, power spectra and the spectra of Lyapunov exponents of the system. The nonlinear dynamics for $M=3$ has also been considered more recently [17,18]. For $M=3$, symmetry arguments show that the dynamics is that of an area-preserving two-dimensional map. As a result, it provides a rich behavior, which is of interest for both theory and experiment of BEC. When $M=3$, the passage of a trajectory from one sto-

chastic region in phase space to another is blocked by Kolmogorov-Arnold-Mosen (KAM) surfaces [19]. When $M>3$, however, Arnold diffusion can take place, that is, in the phase space of the system, stochastic layers of different resonances intersect. Therefore, the motion will spread out over the entire system of intersecting layers [19]. Arnold conjectured that this instability is generic to higher-dimensional nonlinear Hamiltonian systems. Indeed, in the context of DNLSE, Arnold diffusion was considered for $M=4$ [20].

In this work, we study different types of chaotic solutions of the DNLSE with periodic boundary conditions and a single on-site defect. In a recent article [21] we have given a global picture of the dynamics of this system. In the current paper we focus on the transition to global stochasticity, where the single one-site defect induces interesting complex dynamics. The number of condensates, $M=7$, allows for the manifestation of phenomena such as Arnold diffusion [19]. The present study of the dynamical properties of this model is carried out considering the Poincaré section in the parameter region of the on-site defect. Moreover, we found several families of stationary solutions. Relevant information on the dynamics was found using suitable return maps of the Poincaré cycles, which, to the best of our knowledge, is considered for the first time in multidimensional conservative systems. These Poincaré cycles allowed us to have a better understanding of the robust properties of this system, which have, we believe, physical relevance. For instance, in continuous time, the population inversions of certain pairs of condensates occur almost simultaneously. That is, these population inversions synchronize in an information sense [21,22]. We systematically study three different routes that lead to this behavior. Moreover, the statistics of these Poincaré cycles display, surprisingly, an almost Markovian behavior in spite of the fact that the condensates are to a good extent phase locked and, therefore, the system shows coherent motion. In fact, a good interference between the matter waves of the condensates is the hallmark of phase locking.

This article has seven sections. The DNLSE and the initial conditions are discussed in Sec. II. In Sec. III, we introduce two types of qualitatively different instabilities induced by the single on-site defect, and we define a suitable Poincaré section. Chaotic symbolic synchronization between spatially symmetric pairs of condensates is also discussed. The onset of chaotic self-trapping as a precursor of chaotic symbolic synchronization is considered in Sec. IV. Two different branches of stationary solutions are considered in Sec. V, where certain bifurcations trigger the onset of the aforementioned symbolic synchronization. In Sec. VI, we discuss the phase locking effect between condensates and the resulting local interference. Finally, in Sec. VII, we give our conclusions.

II. THE MODEL AND THE INITIAL CONDITIONS

We consider a one-dimensional ring of coupled BECs. When the height of the interwell barriers is much larger than the chemical potential of the system, the latter corresponds to an array of weakly coupled condensates, whose equation of motion [6] is given by

$$i\frac{\partial \Psi_m}{\partial t} + \Delta_m \Psi_m + K(\Psi_{m-1} + \Psi_{m+1}) + \rho|\psi_m|^2\Psi_m = 0, \quad (1)$$

where Ψ_m stands for the condensate complex amplitude in the mth well, ρ is the nonlinear coefficient arising from the interatomic interaction, K is proportional to the microscopic tunneling rate between adjacent sites, Δ_m stands for the on-site defect and is proportional to an external field superimposed on the lattice, and, finally, t is the time. By introducing the dimensionless amplitude $\psi_m=\sqrt{\rho/2K}\Psi_m \exp[-i(\Delta+2K)t]$, Eq. (1) transforms into the discrete nonlinear Schrödinger equation given by

$$i\frac{\partial \psi_m}{\partial \tau} + \delta_m \psi_m + (\psi_{m-1} + \psi_{m+1} - 2\psi_m) + 2|\psi_m|^2\psi_m = 0, \quad (2)$$

where $\delta_m=(\Delta_m-\Delta)/K$ stands for the defects, $\tau=Kt$, and Δ is any arbitrary number. As a result, the only parameters of the DNLSE in Eq. (2) correspond to the defects δ_m. The system is assumed to have periodic boundary conditions. The positive sign before the nonlinear term indicates that we are considering an attractive interatomic interaction between the condensates, such as in the case of lithium atoms [23].

There are two integrals of motion in Eq. (2). The first is the Hamiltonian, from which Eq. (2) is derived [1]. It is given by

$$H = \sum_{m=1}^{M} (|\psi_m - \psi_{m+1}|^2 - |\psi_m|^4 - \delta_m|\psi_m|^2). \quad (3)$$

The second constant is the norm, which is given by

$$N = \sum_{m=1}^{M} |\psi_m|^2. \quad (4)$$

Here M stands for the number of condensates.

We can rewrite the DNLSE by transforming into action-angle variables (N_m, θ_m), where $\psi_m=\sqrt{N_m}\exp(-i\theta_m)$, to stress the physical meaning of the equations of motion. The equations for $N_m \geqslant 0$ and θ_m are the following:

$$\frac{dN_m}{d\tau} = 2\sqrt{N_m N_{m-1}}\sin(\theta_{m-1}-\theta_m) + 2\sqrt{N_m N_{n+1}}\sin(\theta_{m+1}-\theta_m),$$

$$\frac{d\theta_m}{d\tau} = 2 - \delta_m - \sqrt{\frac{N_{m-1}}{N_m}}\cos(\theta_{m-1}-\theta_m) - \sqrt{\frac{N_{m+1}}{N_m}}\cos(\theta_{m+1} - \theta_m) - 2N_m. \quad (5)$$

We will see that, in the chaotic regimes that we study, the inequality $|\theta_m-\theta_n| \ll 1$ holds, and therefore the system is phase locked [24]. N_m stands for the population of site m.

We will use as initial conditions a set of stationary solutions which arise when the defect parameter is given by $\delta_m=0$ [21,25]. To find these DNLSE stationary solutions, we use the nonlinear map approach [26,27]. This map is obtained by setting $dN_n/d\tau=0$, and $\theta_n=\theta_m$, for any $n\neq m$ in Eq. (5). Moreover, we can define the frequency of the resulting periodic orbit by setting $d\theta_m/d\tau=\lambda$, where λ is a constant.

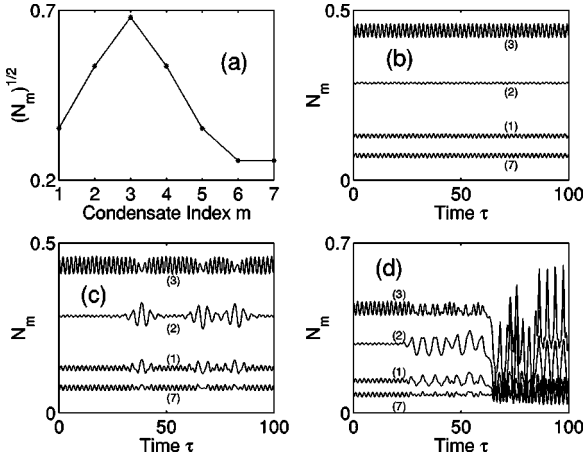

FIG. 1. (a) Plot of stationary solution amplitude $\sqrt{N_m}$ versus condensate index m where $\Gamma=2.5$. Plot of N_m versus time τ for δ_3 = (b) -0.005, (c) -0.0065, and (d) -0.007. The labels 1, 2, 3, and 7 are the condensate indices. The variable τ has been further rescaled by dividing by 4π.

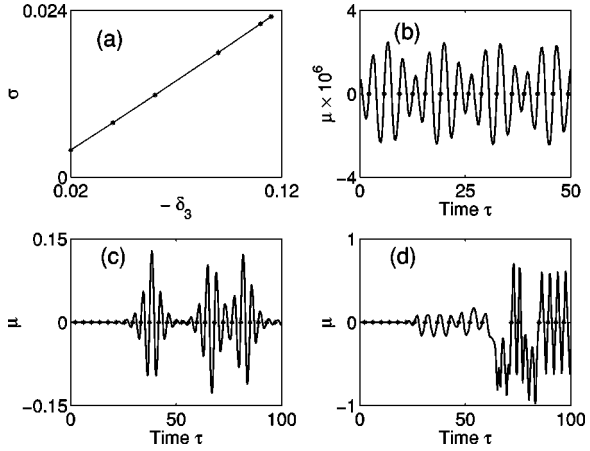

FIG. 2. (a) Distance σ versus $-\delta_3$. Plot of μ versus time τ for δ_3= (b) -0.005, (c) -0.0065, and (d) -0.007.

Therefore, the stationary solutions have the form $\psi_m(\tau) = \sqrt{N_m}\exp(-i\lambda\tau)$. As a result, the following cubic map (CM) is obtained:

$$X_{n+1} = Y_n,$$

$$Y_{n+1} = (\Gamma_n - 2Y_n^2)Y_n - X_n, \tag{6}$$

where $\Gamma_n=2-\lambda-\delta_n$ and $Y_n=\sqrt{N_n}$. In the CM we will set $\Gamma_n=\Gamma=2-\lambda$ for which $\delta_n=0$. The Jacobian J of this map is area preserving, i.e., $J=1$. The fixed points $(\pm\sqrt{\Gamma/2-1}, \pm\sqrt{\Gamma/2-1})$ of the CM are elliptic for $2<\Gamma<4$. When $\Gamma=2.5$, we find a period-7 orbit surrounding the elliptic fixed point. The periodic orbit is surrounded by island chains [25]. We will consider those stationary solutions of the DNLSE that are determined by the (elliptic) stable periodic orbits of the CM. Such a periodic orbit with periodicity 7 generates linearly stable stationary solutions in a ring with seven condensates. The amplitudes of this stationary solution are shown in Fig. 1(a).

III. DEFECT-INDUCED OSCILLATIONS AND THE POINCARÉ SECTION

From here on we consider the DNLSE with a single defect, $\delta_3<0$, and $\delta_n=0$ for $n\neq 3$, in a ring with seven condensates. We make use of the exact stationary DNLSE solution of the previous section as initial condition for this perturbed DNLSE. This contrasts with a previous article [21], where we added small random perturbations of the order of 10^{-3} to the initial conditions to test for the stability and robustness of the solutions. Keeping the initial condition fixed allows us to study the onset of chaos as the defect parameter is changed. As the parameter $\delta_3<0$ increases in absolute value, we find a transition from a quasiperiodic solution to a chaotic solution where the oscillations of N_m are localized within a small neighborhood of the stationary solutions. These regimes are observed in Figs. 1(b) and 1(c), for which $\delta_3=-0.005$ and $-0.006\,25$, respectively. These localized chaotic oscillations occur in a narrow interval $-0.0069<\delta_3<-0.0055$ and are not typical when $\delta_3<0$. In contrast, the presence of a defect $\delta_3>0$, in the quasiperiodic or chaotic regime, typically induces localized oscillations of N_m [21]. The localized solutions are referred to as self-trapping solutions [17,18,20]. As the parameter $\delta_3<0$ decreases further, we find a typical scenario where the oscillations of N_m become delocalized, as observed in Fig. 1(d). Here, the initial behaviour of N_m is characterized by time sequences, that are reminiscent of quasiperiodic and localized chaotic motions.

In order to measure the extent of localization in the DNLSE, the quantity $\eta=-[1/\ln(M)]\Sigma_{i=1}^{M}(\langle N_i\rangle/N)\ln(\langle N_i\rangle/N)$ has been used when $M=3$ [17]. $\langle\,\rangle$ stands for the sample average or mean, and M is the number of condensates. The quantity η is unity when the populations N_i are the same on average, and is zero in the limit when only one of the populations N_i is different from zero. In the chaotic self-trapping regime, when $\delta_3=-0.006\,25$, we find that $\eta\approx 0.9056$. As a reference we can consider the stationary solution when $\delta_3=0$, where we obtain $\eta\approx 0.88$. However, when $\delta_3=-0.007$, the continuous-time chaotic delocalized solutions give $\eta\approx 0.9905$. As a result, the populations of the condensates N_i have almost the same mean. When $M=3$, chaos usually leads to $\eta\approx 1$ for relatively small constants of motion N [17]. In these different oscillatory regimes, the change of $\delta_3<0$ induces an increment of the distance from $U(\delta_3)$, the stationary solution when $\delta_3<0$, to the fixed initial condition $U(0)=(\sqrt{N_1},\sqrt{N_2},\sqrt{N_3},\sqrt{N_4},\sqrt{N_5},\sqrt{N_6},\sqrt{N_7})$, the stationary solution when $\delta_3=0$, shown in Fig. 1(a). The distance between these two points is given by $\sigma\equiv|U(\delta_3)-U(0)|$. The dependence of σ on $\delta_3<0$ is approximated by $\sigma\approx -2\delta_3+C$, where C is a constant. This is shown in Fig. 2(a). We have found these central resonances $U(\delta_3)$, when $\delta_3<0$, using a root finding scheme with initial guesses in the vicinity of $U(0)$, the stationary solution at $\delta_3=0$.

The picture that emerges is, therefore, that of an initial condition, given in Fig. 1(a), moving away from the central resonance $U(\delta_3)$, as shown in Fig. 2(a). As in any Hamiltonian system, this leads to a closer vicinity to the stochastic layers where chaotic behavior occurs. Moreover, since the

number of degrees of freedom of our system is larger than 2, these stochastic layers are expected to form an interconnected network, which is known as an Arnold web [19]. The thickness of these layers, typically, expands with increasing perturbation [19]. This is observed when we decrease the parameter $\delta_3<0$ in the interval $-0.0069<\delta_3<-0.0055$. In fact, the time series of N_m, in Fig. 1(c), increase their oscillation amplitudes with decreasing $\delta_3<0$. At a given point, however, when the thickness of these layers is wide enough, resonance overlap and motion across certain stochastic layers occurs, leading to the onset of a stronger chaotic motion. This is precisely what one sees in Fig. 1(d). We will return to this issue below, considering a suitable Poincaré section.

Let us define the new variable $\mu \equiv N_L - N_R$, where $N_L = N_7 + N_1 + N_2$ and $N_R = N_4 + N_5 + N_6$ are the left and right wing populations, respectively. In the quasiperiodic, self-trapping chaotic, and delocalized chaotic regimes, the trajectory intersects an 11-dimensional surface $\mu=0$ transversally, as suggested by Figs. 2(b), 2(c), and 2(d). $\mu=0$ defines an 11-dimensional surface due to the existence of the constants of motion H and N. The Poincaré surface of section is defined to be where the trajectory intersects this surface from $\mu<0$ to $\mu>0$, as shown in Fig. 2, that is, when $\mu=0$ and $d\mu/d\tau > 0$. The associated map of a Hamiltonian flow is also area preserving [19]. Since the DNLSE is a Hamiltonian flow with two constants of motion, there are four Floquet multipliers equal to 1 for each periodic orbit [19]. As a result, the associated volume-preserving map is ten dimensional when $M=7$. Similarly, the corresponding map becomes two dimensional when $M=3$. These four Floquet multipliers imply the presence of four vanishing Lyapunov exponents in the DNLSE.

Let us consider first the self-trapping chaotic regime for which $\delta_3=-0.006\,25$. At the Poincaré section, we find that $|N_1-N_5|\sim 10^{-3}$, $|N_2-N_4|\sim 10^{-3}$, and $|N_6-N_7|\sim 10^{-3}$. Therefore, taking into account the typical magnitudes of N_m from Fig. 3(a), we have that $N_1\approx N_5$, $N_2\approx N_4$, and $N_6\approx N_7$ at the Poincaré section. In the case where $\delta_3=-0.007$, the population differences N_1-N_5, N_2-N_4, and N_6-N_7 have the same sign most of the time, as is clearly appreciated in Figs. 3(c) and 3(d). Thus, these population differences, to a significant extent, undergo inversion at the same time and have the same sign of $\mu \equiv N_R - N_L$. The characteristic magnitudes of the population inversions N_1-N_5, N_2-N_4, and N_6-N_7 at the Poincaré section and at their maxima differ by almost two orders of magnitude when $\delta_3=-0.007$. Moreover, this behavior seems to be robust, as confirmed by extensive numerical simulations. This is precisely what makes this continuous-time synchronous inversion relevant, we believe, from an experimental standpoint.

The behavior when $\delta_3=-0.007$ is an example of synchronization of symbolic information (SSI), and holds, at least, for time units as large as $\tau\sim 10^5$. According to this notion, two arbitrary oscillators are perfectly synchronized in an information sense if they produce the same information at the same rate, i.e., symbols generated by one system map one-to-one to symbols emitted by the other system [28,29]. Strictly speaking, this form of synchronization requires that the common information be emitted at precisely the same time. Figures 3(c) and 3(d) suggest that the population inversions exhibit almost equivalent information at the same average rate. In our Hamiltonian system, we compare the symbolic dynamics of these three chaotic population inversions.

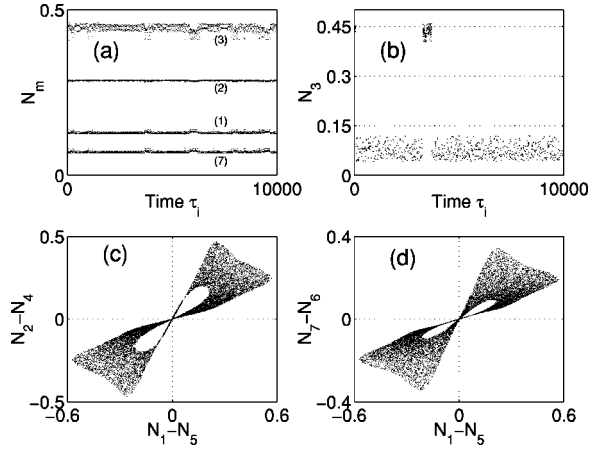

FIG. 3. (a) Plot of N_m versus time τ_i at the Poincaré section when $\delta_3=-0.0065$. The labels 1, 2, 3, and 7 are the condensate indices. (b) Plot of N_3 versus time τ_i when $\delta_3=-0.007$ at the Poincaré section. (c) Plot of N_2-N_4 versus N_1-N_5 when $\delta=-0.007$ for continuous time. (d) Plot of N_7-N_6 versus N_1-N_5 when $\delta=-0.007$ for continuous time.

IV. CHAOTIC SELF-TRAPPING AS A PRECURSOR OF SSI

We now focus on the dynamics in the Poincaré section. The time series of N_m, when $\delta_3=-0.0065$ and -0.007, are shown in Figs. 3(a) and 3(b), respectively. Figure 3(a) suggests that in the self-trapping regime there is some underlying fine structure in the dynamics, which is more clearly appreciated for N_3. Instead, Fig. 3(b) suggests that there is no such structure when $\delta_3=-0.007$ and, moreover, this figure shows that the trajectory has been in the self-trapping region roughly during the time intervals $0<\tau_i<60$ and $3200<\tau_i<3600$. In fact, in a high-precision calculation consisting of 10^5 time units, only these jumps between these two chaotic regions have taken place. The variable τ has been rescaled by dividing by 4π.

We show evidence suggesting that the dynamics when $\delta_3=-0.0065$, to some extent, consists of a sequence of motions along the stochastic layers of different resonances. To support this, we address the dynamics shown in Fig. 4. We have considered the Poincaré cycles $\tau_{i+1}-\tau_i$ as return maps. The indices i label consecutive Poincaré sections and τ_i is the Poincaré recurrence time [19]. In Fig. 4(a), the motion wanders stochastically around a multiple resonance of period 5. In fact, if we sample this map each five Poincaré sections, we only see a single stochastic layer. This occurs in the interval $2700<i<3900$. Figure 4(b) suggests that the associated resonance is of period 7. Figure 4(c) indicates that the orbit is in the neighborhood of a resonance torus of period 12. This seems to be a secondary generation resonance where the primary has period 3. Figure 4(d) suggests that the related resonance is a simple resonance. The intervals of the indices i of Figs. 4(b), 4(c), and 4(d), are $8580<i<8670$, $6600<i$

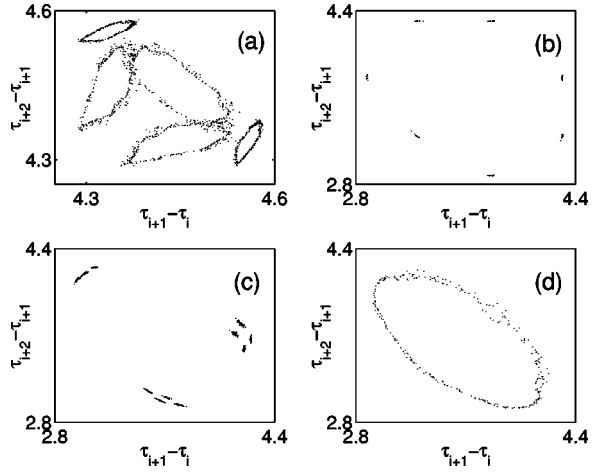

FIG. 4. Return map of the Poincaré cycles, that is, $\tau_{i+2}-\tau_{i+1}$ versus $\tau_{i+1}-\tau_i$ when $\delta_3=-0.0065$ at the Poincaré section for (a) $2700<i<3900$, (b) $8580<i<8670$, (c) $6600<i<7100$, and (d) $5100<i<5380$.

<7100, and $5100<i<5380$, respectively. In Fig. 5(a) we have shown the time series of $\tau_{i+1}-\tau_i$ versus index i for $12\,000<i<26\,000$. During this long time interval the motion sticks to the neighborhood of a period-5 resonance torus as indicated by Fig. 5(b). Indeed, by sampling this time series every five Poincaré sections, we will only see a single stochastic layer. This period-5 resonance is, however, different from that of Fig. 4(a). Therefore, we have seen that the stochastic layers of different resonances are connected and that the trajectory spreads out over this system of intersecting layers. This behavior takes place for time units of τ as large as 10^5 as suggested by Fig. 5.

We believe that these long residence times near resonances can be explained as follows. In Hamiltonian systems with three or more degrees of freedom, a dense set of resonant tori can persist. Generically, the stable and unstable manifolds of each preserved torus intersect transversally yielding a homoclinic tangle. Moreover, the homoclinic

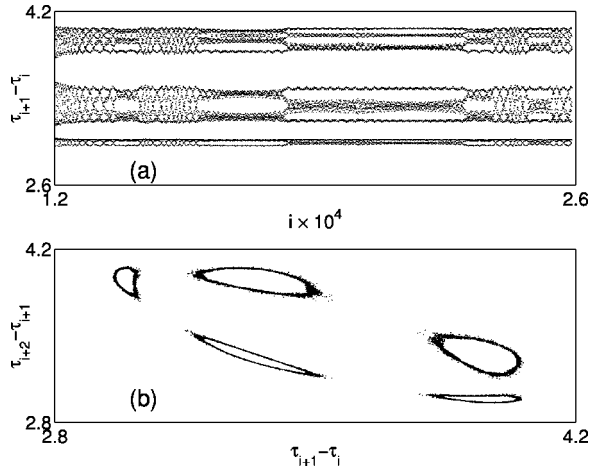

FIG. 5. (a) Plot of the time series of $\tau_{i+1}-\tau_i$ for $12\,000<i<26\,000$ when $\delta_3=-0.0065$. (b) $\tau_{i+2}-\tau_{i+1}$ versus $\tau_{i+1}-\tau_i$ for the time series of (a).

tangle of each torus becomes intertwined with the homoclinic tangles of nearby tori, leading to the possibility that orbits starting near any one of these tori may diffuse along this dense set of homoclinic tangles in a chaotic fashion [33]. This is at the heart of what is known as Arnold diffusion [19].

Figures 1(c) and 1(d) suggest that there are orbits having three time scales for the motion: First, a small time scale, where the system looks integrable; second, a widely extended intermediate time scale, where the actions are confined in a bounded domain with a nontrivial dynamics; finally, a long time scale, where the motion is no longer local and, seemingly, all the degrees of freedom are involved [30]. The second stage of evolution can be supported by the Nekhoroshev theorem. In this theorem, where the evolution of the system is considered only for finite (but large) times, one obtains estimates which are valid in small neighborhoods of phase space for the variations of the action variables [31]. Nekhoroshev considers a quasi-integrable Hamiltonian, where the perturbation to the integrable part of the Hamiltonian is small enough. Moreover, if this integrable part is convex then the actions are confined in a small neighborhood during an exponentially long time, which increase exponentially with the smallness of the perturbation [31].

To apply this theorem to the Hamiltonian H, which is given in Eq. (3), we have to show that the integrable part, which we label as $H_0(N_1,N_2,\ldots,N_M)$, is convex. Here we have to make use of $N=\Sigma_{i=1}^{M}N_i$, the second constant of motion. That is, we need to show that the Hessian matrix of $H_0(N_1,N_2,\ldots,N_M)$ is definite in a vicinity of the initial conditions. To obtain $H_0(N_1,N_2,\ldots,N_M)$, we have replaced $\psi_m=\sqrt{N_m}\exp(-i\theta_m)$ in Eq. (3) and, moreover, we have considered the term with the factor δ_3 as a small perturbation. In addition, on the basis of our numerical simulations, we assume that $|\theta_m-\theta_n|\ll 1$ is valid for the long time scales considered in this theorem. These angle differences also correspond to a small perturbation. Upon these considerations, the Hamiltonian H_0 takes the form

$$H_0=\sum_{m=1}^{M}[(\sqrt{N_m}-\sqrt{N_{m+1}})^2-N_m^2]. \tag{7}$$

When $M=7$, the Hessian of the Hamiltonian H_0 depends on six actions, since the constant N has been taken into account. The evaluation of the Hessian, at the stationary solution of Fig. 1(a), gives the spectrum of eigenvalues ν_n, after replacing N_7 in H_0. These are $\nu_1=0.1148\ldots$, $\nu_2=0.1933\ldots$, $\nu_3=3.8664\ldots$, $\nu_4=6.8310\ldots$, $\nu_5=15.6296\ldots$, and $\nu_6=126.7421\ldots$. Observe that these eigenvalues have the same sign. This suggests that the Hamiltonian H_0 is convex in the neighborhood of the aforementioned initial conditions. As a result, the conditions of the Nekhoroshev theorem appear to hold in our simulations and what we see in Fig. 1(c) is the Nekhoroshev regime, where the actions N_m are bounded in a small neighborhood allowed by the two conservation laws. A similar set of eigenvalues is obtained if we replace any of the actions N_m, instead of N_7, in H_0.

As we decrease the negative parameter δ_3 further, the oscillation amplitudes of N_m expand slightly, leading, for a

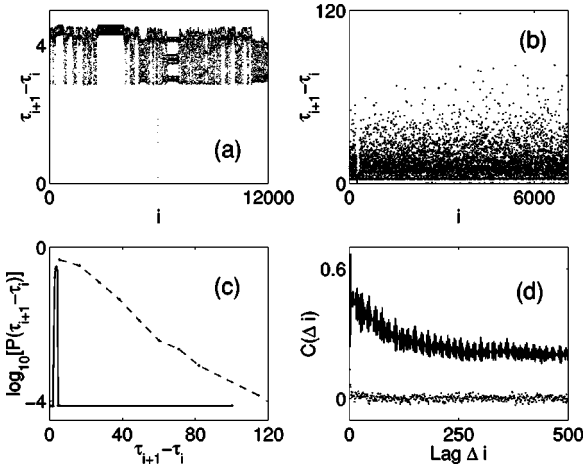

FIG. 6. Plot of $\tau_{i+1}-\tau_i$ versus the Poincaré section index i when δ_3= (a) -0.0065 and (b) -0.007. (c) Plot of $\log_{10}P(\tau_{i+1}-\tau_i)$ for $\delta_3=-0.0065$ (continuous line) and -0.007 (dashed line). (d) Plot of the ACF $C(\Delta i)$ for $\delta_3=-0.0065$ (continuous line) and -0.007 (dots).

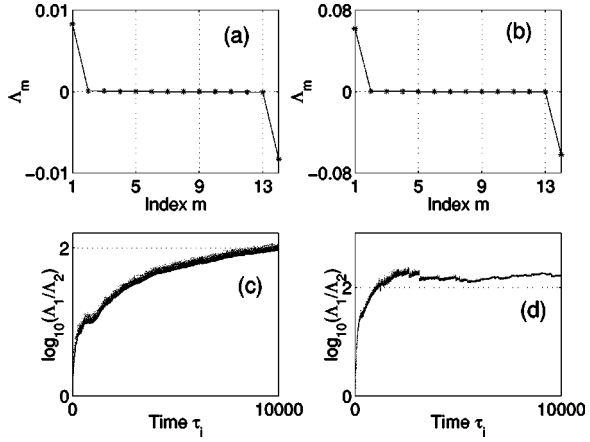

FIG. 7. Plot of the Lyapunov exponents Λ_m versus index m for δ_3= (a) -0.0065 and (b) -0.007. Plot of $\log_{10}(\Lambda_1/\Lambda_2)$ versus time τ_i for δ_3= (c) -0.0065 and (d) -0.007.

given parameter δ_3, to the onset of a stronger stochastic motion in a larger region as shown in Figs. 1(d), 3(c), and 3(d). Moreover, we see that when SSI takes place, in spite of the small change of δ_3, the largest Lyapunov exponent increases several times. This qualitative change can be understood as the overlap of certain resonances which belong to different regions of phase space. The self-trapping chaotic regime, when $\delta_3=-0.0065$, can also be affected if the region contains a large amount of KAM tori, which act as effective barriers for limiting large excursions of chaotic orbits [32]. Instead, for $\delta_3=-0.007$, these barriers no longer operate, due to the overlapping of certain resonances and, therefore, the orbit can explore both the region of self-trapping and that of SSI, as observed in Fig. 3(b).

To have a quantitative measure of the stochasticity, we consider the time series of $\tau_{i+1}-\tau_i$ as well as the spectra of the Lyapunov exponents of the system. The time series $\tau_{i+1}-\tau_i$ when $\delta_3=-0.0065$ is narrow, sharply bounded, and has time intervals with some regularity, as shown in Figs. 5(a) and 6(a). These intervals are typically generated by the motion around a given resonance torus. Instead, when $\delta_3=-0.007$ there are no signs of such a regularity. In fact, the time series looks quite noisy, as shown in Fig. 6(b). The probability distribution function (PDF) of the Poincaré cycles $\tau_{i+1}-\tau_i$ is sharply peaked and bounded when $\delta_3=-0.0065$, while the core of this PDF, when $\delta_3=-0.007$, has to a good extent a broad exponential dependence. These PDFs are shown in Fig. 6(c). We stress that the exponential dependence of this PDF core indicates that these Poincaré cycles have, to a good degree, a Markovian character. In other words, in case we have a perfect Markovian process [34], the probability that the trajectory continues with a given symbol of μ until $\tau^{**}>\tau^*$ is independent of the past duration $\tau^*-\tau_i>0$, where $\tau^{**}<\tau_{i+1}$. Here, τ_i is the last time that the trajectory intersected the Poincaré surface of section. The prevalent Markovian character of this time series implies small memory. This is precisely what we show below by calculating the autocorrelation function (ACF) $C(\Delta i)$ for these time series, where $C(\Delta i)=\Sigma_{i=1}^{i=R-S}(\Delta\tau_i-\Delta\tau)(\Delta\tau_{i+\Delta i}-\Delta\tau)/\Sigma_{i=1}^{i=R-S}(\Delta\tau_i-\Delta\tau)^2$. In this equation, $\Delta\tau_i=\tau_{i+1}-\tau_i$ and $\Delta\tau$ are the time series and its sample average, respectively. Δi is the time lag, R is the number of data points, $\Delta i<S$, and $R\gg S$ [19]. The ACF $C(\Delta i)$ of $\tau_{i+1}-\tau_i$ for the time series of Fig. 6(a) has a slow nonexponential decay, when $\delta_3=-0.0065$, as a result of the presence of intervals with some regularity. Instead, the ACF $C(\Delta i)$ has a fast decay which implies a small memory for the time series of Fig. 6(b), as indicated on the basis of the aforementioned exponential dependence. The plots of these ACFs $C(\Delta i)$ are shown in Fig. 6(d). However, there are, besides some fitting arguments, at least two reasons that make the time series of Fig. 6(b) somewhat different from a Markovian process. First, there is the presence of temporal jumps to the self-trapping region, where the motion is highly correlated, as suggested by Fig. 3(b). The second is the existence of very long time intervals $\tau_{i+1}-\tau_i$ that appear as rare events. The latter arise in the tails of our PDF and, typically, have power law dependence [35]. These are not shown in the dashed line of of Fig. 6(c) since its probability is negligible, at least during our time series consisting of 10^5 time units. It should be underlined that, in spite of this quasi-Markovian behavior, certain pairs of condensates can synchronize the symbolic dynamics of their population inversions. This is related to phase locking, since lack of the latter inhibits the presence of SSI [21].

To verify the stochasticity of the motion, let us consider the spectra of the Lyapunov exponents. These are shown for $\delta_3=-0.0065$ and -0.007 in Figs. 7(a) and 7(b), respectively. The largest positive Lyapunov exponent Λ_1, for $\delta_3=-0.0065$, is almost six times smaller than that when $\delta_3=-0.007$. To understand this, we point out that in the chaotic self-trapping regime there is some regularity, as appreciated in Figs. 4 and 5. In contrast, when $\delta_3=-0.007$, the system behaves almost like a Markovian process. When both the chaotic self-trapping and SSI take place, there is a single positive Lyapunov exponent whose magnitude is much larger than that of the other positive Lyapunov exponents. The evolution of the ratio between the two largest Lyapunov exponents, Λ_1/Λ_2, for $\delta_3=-0.0065$ and -0.007 is given in Figs.

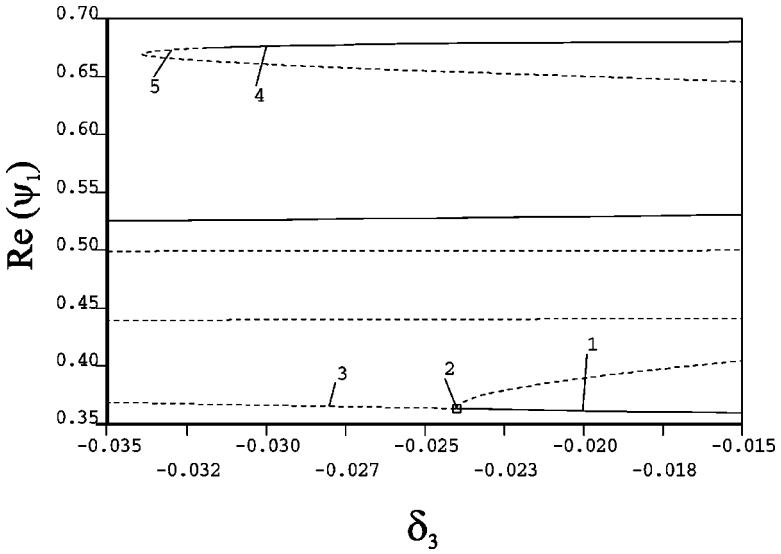

FIG. 8. Plot of the real part of the stationary solution ψ_1 of Eq. (2) versus δ_3. Here the period of the solution, $2\pi/\lambda$, remains constant. See text.

7(c) and 7(d) respectively. As indicated above, the two conservation laws of our autonomous Hamiltonian system imply that we have at least four Lyapunov exponents which are equal to zero.

V. FAMILIES OF STATIONARY SOLUTIONS

We have carried out a numerical study of stationary solutions for the case of a ring with seven condensates. Partial results are shown in Fig. 8, where the real part of the stationary solution ψ_1 is shown versus the parameter δ_3. Evidently, there are many stationary solutions in the indicated parameter range. The solution point with label 2 in Fig. 8 corresponds to a branch point (or pitchfork bifurcation). Solid curves denote (linearly) stable stationary solutions, while dashed curves denote unstable solutions. The period of the stationary solutions, $2\pi/\lambda$, along the two bifurcation branches remains constant. In the neighborhood of the stable stationary solutions, just before the bifurcations, the dynamics is quasiperiodic, such as near the stationary solutions with labels 4 and 1. Instead, just after the bifurcation points, initial conditions in the vicinity of the unstable stationary solution trigger the onset of the chaotic dynamics, such as near the stationary solutions with labels 3 and 5, where $\delta_3^{(3)} = -0.028$ and $\delta_3^{(5)} = -0.032\,99$, respectively.

The dependence of the amplitudes $\sqrt{N_m}$ on the the index m for the unstable stationary solution at $\delta_3^{(5)} = -0.032\,99$ is given in Fig. 9(a). In this figure, we can see that the amplitude dependence is not symmetric with respect to the on-site defect position at the index $m=3$, as in the case of Fig. 1(a). However, as shown by Fig. 9(b), SSI takes place to a good degree in the continuous flow. Moreover, at the Poincaré section, we find that $|N_1 - N_5| \sim 10^{-3}$, $|N_2 - N_4| \sim 10^{-3}$, and $|N_6 - N_7| \sim 10^{-3}$. That is, the population inversions at $\mu = 0$ are about a hundred times smaller than their maximum magnitude. A qualitatively similar behavior was observed before for $\delta_3 = -0.007$. Quite a different story is, however, the case for which $\delta_3^{(3)} = -0.028$. Here the dependence of the amplitudes $\sqrt{N_m}$ on the the index m is symmetric as shown in Fig. 9(c); however, the behavior of SSI has been somehow degraded as suggested by Fig. 9(d). In fact, the aforementioned population inversions at $\mu = 0$ are only about ten times smaller than their maximum magnitude and do not change sign in a synchronous way with the accuracy of the previous cases when $\delta_3^{(5)} = -0.032\,99$ and $\delta_3 = -0.007$.

Figure 10(a) suggests that the positive Lyapunov exponent Λ_1 for $\delta_3^{(3)}$ is larger than that for $\delta_3^{(5)}$, where SSI happens with accuracy. Moreover, while the ratio $\Lambda_1/\Lambda_2 \sim 10^2$ for $\delta_3^{(5)}$, $\Lambda_1/\Lambda_2 \sim 1$ for $\delta_3^{(3)}$. In fact, from previous calculations we know that lack of SSI implies that the nonvanishing Lyapunov exponents have roughly the same order. In addition, the cores of the PDF for the Poincaré cycles $\tau_{i+1} - \tau_i$ when $\delta_3^{(5)}$ and $\delta_3^{(3)}$ are shown in Fig. 10(b). Both have roughly an exponential dependence which accounts for the rough Markovian behavior in these time series of $\tau_{i+1} - \tau_i$. We have carried out a study of the bifurcations of the stationary solutions as the parameter δ_3 is changed for different number of condensates M. When $M=6$, the behavior of these

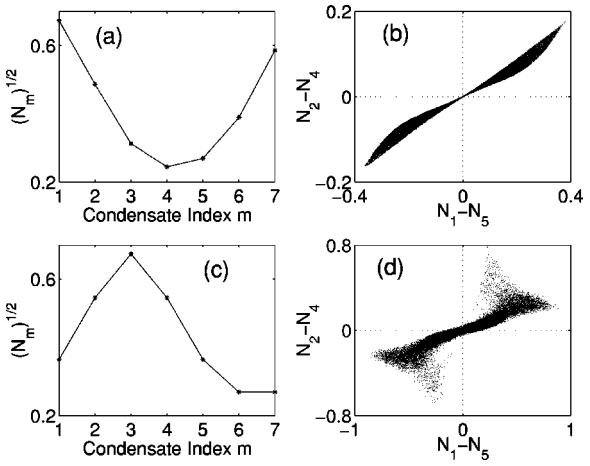

FIG. 9. (a) Plot of stationary solution amplitude $\sqrt{N_m}$ versus condensate index m when $\delta_3 = \delta_3^{(5)}$. (b) Plot of $N_2 - N_4$ versus $N_1 - N_5$ when $\delta = \delta_3^{(5)}$ for continuous time. (c) Same as (a) but for $\delta_3 = \delta_3^{(3)}$. (d) Same as (b) but for $\delta_3 = \delta_3^{(3)}$.

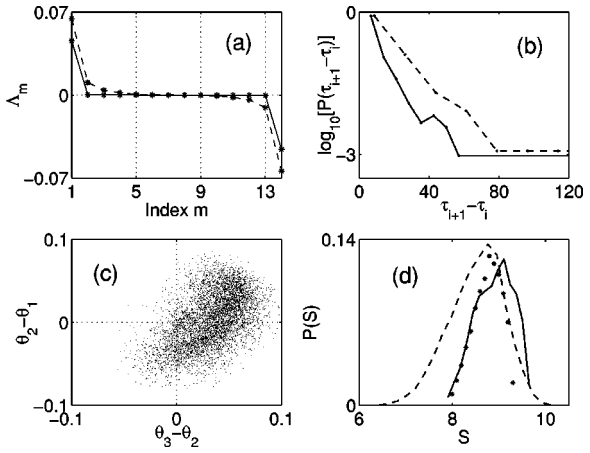

FIG. 10. (a) Plot of the Lyapunov exponents Λ_m versus index m for $\delta_3=\delta_3^{(5)}$ (solid line) and $\delta_3^{(3)}$ (dashed line). (b) Plot of $\log_{10}P(\tau_{i+1}-\tau_i)$ for $\delta_3=\delta_3^{(5)}$ (solid line) and $\delta_3^{(3)}$ (dashed line). (c) Plot of $\theta_3-\theta_2$ versus $\theta_2-\theta_1$ at the Poincaré section when $\delta=-0.007$. (d) Plot of the PDF $P(S)$ for $\delta=-0.007$ (continuous line), $\delta_3^{(5)}$ (dotted line), and $\delta_3^{(3)}$ (dashed line).

stationary solutions is qualitatively similar to that for $M=7$. However, when $M=9$ and 11, the related stationary solutions are unstable within an interval of δ_3 similar to that of the case with $M=7$. Moreover, as expected, these unstable stationary solutions display a richer bifurcation behavior.

VI. PHASE LOCKING AND LOCAL INTERFERENCE

In the tight binding approximation, besides the number of particles in each site, N_m, the relative phases $\theta_m-\theta_{m+1}$ of neighboring condensates are relevant quantities. In fact, these determine the robusteness of a constructive interference pattern [23,36]. We show below that phase locking takes place in our model, i.e., $|\theta_m-\theta_{m+1}|<2\pi$ for all m [24]. It should be emphasized that lack of a significant degree of phase locking inhibits the presence of SSI, as discussed elsewhere [21]. A good interference pattern arises, however, only when $|\theta_m-\theta_{m+1}|\ll 1$. It is remarkable that when chaos arises, in the form of self-trapping or SSI, we find that $|\theta_m-\theta_n|\ll 1$, in spite of the fact that nearby trajectories diverge exponentially fast. Indeed, when $\delta_3=-0.0065$ we have obtained that $|\theta_m-\theta_n|<10^{-2}$. Instead, in Fig. 10(c), where $\delta_3=-0.007$, we show that $|\theta_m-\theta_n|<10^{-1}$.

The value of the Hamiltonian H in Eq. (3) can be approximated when $\delta_3=-0.0065$ at any time by

$$H_1=\sum_{m=1}^{M}(\sqrt{N_m}-\sqrt{N_{m+1}})^2-N_m^2-\delta_m N_m. \tag{8}$$

Defining the parameter $\alpha_1\equiv(H_1-H)/H$, we find that $0<\alpha_1<10^{-3}$. Now, we can make use of the definition of the Poincaré section to find that $N=2N_1+2N_2+2N_7+N_3$ is conserved when $\mu=0$. Our simulations suggest that, at the Poincaré section, we can replace $N_4\to N_2$, $N_5\to N_1$, and $N_6\to N_7$ in the expression for H_1. As a result, for the value of H, we get the following approximate expression:

$$H_2=2(N-N_7-2\sqrt{N_1N_2}-2\sqrt{N_2N_3}-2\sqrt{N_1N_7})-2N_1^2-2N_2^2-2N_7^2-N_3^2-\delta_3N_3. \tag{9}$$

N_7 can be eliminated using, at the Poincaré section, the identity $N=2N_1+2N_2+2N_7+N_3$. Defining now the parameter $\alpha_2\equiv(H_2-H)/H$, we find that $|\alpha_2|<3\times10^{-4}$ when $\delta_3=-0.0065$. In Eq. (9), H_2 is a two-dimensional surface embedded in a three-dimensional space (N_1,N_2,N_3), provided that H_2 is constant. Since H_2 is preserved to a good extent, we can qualitatively explain why the spectrum of the Lyapunov exponents has approximately a single positive Lyapunov exponent as suggested by Fig. 7(a). Therefore, it appears that there is a two-dimensional map on the aforementioned surface in the space (N_1,N_2,N_3), which approximately emulates the dynamics of our system at the Poincaré sections. A chaotic orbit of this map would give two Lyapunov exponents, which can be related to the largest, in absolute value, Lyapunov exponents of Fig. 7(a). The remaining nonvanishing Lyapunov exponents are negligible when compared to the largest one, as suggested by Fig. 7(c). We underline, however, that, by no means, does our system have the dynamics of a two-dimensional map. We have shown evidence of motion along different resonances, which we believe is, at least, partially due to Arnold diffusion. The latter was also supported by the apparent fulfilment of the conditions of the Nekhoroshev theorem when $\delta_3=-0.0065$.

One of the manifestations of the wave nature of Bose-Einstein condensates is the observation of interference when the condensed and initially separated clouds of atoms are allowed to overlap [12]. This is carried out in the experiments by turning off, after different evolution times, both the magnetic and optical traps. Therefore, upon expansion the condensates overlap and interfere, and if the effects of particle interactions in the overlap region can be neglected, the particle density at any point on the central axis of the ring of atoms, which is perpendicular to the plane of the ring, is proportional to

$$S(\tau)=\left|\sum_{m=1}^{M}\psi_m\right|^2. \tag{10}$$

If $S(\tau)$ is measured just after the traps are turned off at τ, we can have an idea of the dynamics by considering several evolution times τ of the system. Since the phase differences satisfy $|\theta_m-\theta_{m+1}|\ll 1$, we can approximate $S(\tau)$ as follows:

$$S_1(\tau)=\left(\sum_{m=1}^{M}\sqrt{N_m}\right)^2. \tag{11}$$

Indeed, $S(\tau)$ approximates $S_1(\tau)$ with good accuracy. Moreover, we further assume that the measurement times τ, where the traps are turned off, are distributed uniformly over a large enough span of time for many replicas of the same experiment having only different τ. In this case, the probability distribution function of S, which we label as $P(S)$, will have a relatively small width when SSI takes place. This is the case when $\delta_3=-0.007$ and $\delta_3=\delta_3^{(5)}$. However, when SSI occurs to a smaller degree, such as when $\delta_3=\delta_3^{(3)}$, the PDF $P(S)$

will have a broader width with larger tails. In this latter case, we find that $|\theta_m - \theta_{m+1}| \sim 1$.

To assess the possibility of an experiment to detect SSI, let us consider Eq. (1) for which the particle's conservation law takes the form $N_{\mathrm{tot}} = \Sigma_{m=1}^{M} |\Psi_m|^2$. Here N_{tot} stands for the total number of atoms in the experiment. Moreover, since $|\psi_m| = \sqrt{\rho/2K}|\Psi_m|$, we get the expression $\zeta(\Sigma_{m=1}^{M}|\psi_m|^2) = 1/2$, where $\zeta \equiv K/\rho N_{\mathrm{tot}}$. From Fig. 1(a), we obtain that $\Sigma_{m=1}^{7}|\psi_m|^2 \approx 1.5$ and, therefore, $\zeta \approx 1/3$. Buonsante, Franzosi, and Penna [18] suggest that the range $0 < \zeta < 4$ is suitable for a physical experiment consisting of a ring with three condensates. Our estimates, $K \approx 0.07 E_R$ and, roughly, 1000 atoms in each well, are taken from Ref. [11], where E_R stands for the recoil energy. Taking into account the population distribution in each well, we get $\rho \approx 10^{-4} E_R$. Moreover, we find that the estimate $\Delta_3 = \delta_3 K \sim 0.000\,45 E_R$ can generate SSI. This value of Δ_3 is realistic in experiments with microtraps, where also the regime of weakly coupled condensates can be achieved with suitable interwell barriers [14]. This defect value for Δ_3 has the order of magnitude of the parabolic external potential in experiments with Josephson junction arrays realized with atomic Bose-Einstein condensates [11].

VII. CONCLUSIONS AND DISCUSSION

We have studied a family of chaotic solutions in a system consisting of a ring of seven weakly coupled BECs with attractive interactions described by the DNLSE. The initial conditions are determined by the stable periodic orbits of a suitable Hamiltonian map. The onset of the chaotic solutions has been systematically considered by changing the on-site defect and, also, by studying a suitable Poincaré map of the system. This allowed us to gain further insight into the dynamics of this system. In particular, the consideration of return maps of successive Poincaré cycles has been useful to describe the dynamics of our system which, to our knowledge, represents an original example of the usefulness of these return maps to study the evolution of many-dimensional Hamiltonian systems.

For a small negative on-site defect, the system undergoes first a transition from the quasiperiodic regime to a chaotic self-trapping regime as the defect $\delta_3 < 0$ is decreased. Next, a transition from the chaotic self-trapping regime to a chaotic regime displaying synchronization of symbolic information, among the populations inversions of different pairs of condensates, occurs as $\delta_3 < 0$ is decreased further. These populations have, however, the same mean. We have shown that the change of the parameter $\delta_3 < 0$, to reach the chaotic self-trapping regime, induces an effective displacement of the initial conditions from the central resonance corresponding to a given defect $\delta_3 < 0$. Once the chaotic self-trapping regime sets in, it is characterized by relatively small fluctuations of the populations of the condensates. Moreover, the dynamics consists mostly of a sequence of motions along the stochastic layers of different resonances, as suggested by the return maps of successive Poincaré cycles. We attribute this behaviour mainly to Arnold diffusion. This is also suggested by the theorem of Nekhoroshev, whose conditions are satisfied in our simulations. In contrast, the SSI regime, which is continuous in time, is characterized by large changes of the populations of the condensates. This regime displays small memory effects as suggested by the time series of the Poincaré cycles, which remind us of an almost Markovian process. However, the coherence of the system, related to the good degree of phase locking, is a necessary condition for the onset of SSI. In the self-trapping and SSI regimes, the system has basically a single positive Lyapunov exponent. We have also studied the stationary solutions as the on-site defect undergoes large changes. We find that a pitchfork bifurcation triggers the onset of the SSI dynamics, where the defect is negative. The case of six weakly coupled condensates behaves similarly to the abovementioned case with seven condensates. An increase in the number of condensates, to nine and eleven, gives unstable stationary solutions with complicated bifurcations. Finally, we have seen that the presence of phase locking in the SSI regime induces a sharp distribution of the particle density along a spatial axis of symmetry of the ring of BEC. The present study suggests that the interesting and complex dynamics of the SSI regime can be a good candidate for experimental verification.

ACKNOWLEDGMENTS

We would like to thank Felix Izrailev for his useful comments. We also would like to thank Ennio Arimondo, Aranya Bhattacherjee, and M. Saba for interesting discussions. This work was supported by CONACYT-México and the International Centre for Theoretical Physics (ICTP).

[1] P. G. Kevrekidis, K. O. Rasmussen, and A. R. Bishop, Int. J. Mod. Phys. B **15**, 2833 (2001); M. Johansson and S. Aubry, Nonlinearity **10**, 1151 (1997).
[2] D. N. Christodoulides and R. I. Joseph, Opt. Lett. **13**, 794 (1988).
[3] D. N. Christodoulides, F. Lederer, and Y. Silberberg, Nature (London) **424**, 817 (2003).
[4] A. Scott, *Nonlinear Science: Emergence and Dynamics of Coherent Stuctures*, 2nd ed. (Oxford University Press, New York, 2003).
[5] A. S. Davydov, J. Theor. Biol. **38**, 559 (1973).
[6] A. Trombettoni and A. Smerzi, Phys. Rev. Lett. **86**, 2353 (2001); A. Trombettoni, A. Smerzi and A. R. Bishop, Phys. Rev. E **67**, 016607 (2003).
[7] S. Flach and C. R. Willis, Phys. Rep. **295**, 182 (1998).
[8] D. K. Campbell, S. Flach, and Y. S. Kivshar, Phys. Today **57** (1), 43 (2004).
[9] B. P. Anderson and M. A. Kasevich, Science **282**, 1686 (1998).
[10] M. Greiner *et al.*, Nature (London) **415**, 39 (2002).

[11] F. S. Cataliotti *et al.*, Science **293**, 843 (2001).
[12] M. R. Andrews *et al.*, Science **275**, 637 (1997).
[13] A. Smerzi, S. Fantoni, S. Giovanazzi, and S. R. Shenoy, Phys. Rev. Lett. **79**, 4950 (1997).
[14] H. Ott *et al.*, Phys. Rev. Lett. **87**, 230401 (2001); M. Saba *et al.*, in Proceedings of the 13th International Laser Physics Workshop. LPHYS4, Trieste, Italy, 2004 (unpublished).
[15] D. Hennig and G. P. Tsironis, Phys. Rep. **307**, 334 (1999).
[16] J. C. Eilbeck, P. S. Lomdahl, and A. C. Scott, Physica D **16**, 318 (1985); J. H. Jensen *et al.*, Phys. Lett. **110A**, 429 (1985); S. De Filippo, M. Fusco Girard, and M. Salerno, Physica D **26**, 411 (1987).
[17] K. W. DeLong, J. Yumoto, and N. Finlayson, Physica D **54**, 36 (1991).
[18] L. Cruzeiro-Hansson *et al.*, Phys. Rev. B **42**, 522 (1990); D. Hennig *et al.*, Phys. Rev. E **51**, 2870 (1995); R. Franzosi and V. Penna, *ibid.* **67**, 046227 (2003); P. Buonsante, R. Franzosi, and V. Penna, Phys. Rev. Lett. **90**, 050404 (2003); M. Johansson, J. Phys. A **37**, 2201 (2004).
[19] A. J. Lichtenberg and M. A. Lieberman, *Regular And Stochastic Motion* (Springer-Verlag, Berlin, 1993).
[20] D. Hennig and H. Gabriel, J. Phys. A **28**, 3749 (1995).
[21] C. L. Pando L. and E. J. Doedel, Phys. Rev. E **69**, 036603 (2004).
[22] C. L. Pando L., e-print nlin/0305011.
[23] F. Dalfovo, S. Giorgini, L. P. Pitaevskii, and S. Stringari, Rev. Mod. Phys. **71**, 463 (1999).
[24] A. Pikovsky, M. Rosenblum, and J. Kurths *Synchronization: A Universal Concept in Nonlinear Sciences* (Cambridge University Press, Cambridge, U.K., 2001).
[25] C. L. Pando L., Phys. Lett. A **309**, 68 (2003).
[26] D. Hennig and H. Gabriel, Phys. Rev. E **57**, 2371 (1998); D. Hennig, K. Rasmussen, H. Gabriel, and A. Bülow, *ibid.* **54**, 5788 (1996).
[27] T. Bountis, H. W. Capel, M. Kollmann, J. C. Ross, J. M. Bergamin, and J. P. van der Weele, Phys. Lett. A **268**, 50 (2000).
[28] A. Shabunin, V. Demidov, V. Astakhov, and V. Anishchenko, Phys. Rev. E **65**, 056215 (2002); M. Palus, V. Komarek, Z. Hrncir, and K. Sterbova, *ibid.* **63**, 046211 (2001).
[29] N. J. Corron, S. D. Pethel, and K. Myneni, Phys. Rev. E **66**, 036204 (2002).
[30] G. Benettin and G. Gallavotti, J. Stat. Phys. **44**, 293 (1986).
[31] P. Lochak and C. Meunier, *Multiphase Averaging for Classical Systems* (Springer-Verlag, New York, 1988).
[32] J. Laskar, Physica D **67**, 257 (1993).
[33] S. Wiggins, *Chaotic Transport in Dynamical Systems* (Springer-Verlag, New York, 1992).
[34] W. Feller, *An Introduction to Probability Theory and Its Application* (Wiley, New York, 1968), Vol. 1.
[35] D. Sornette, *Critical Phenomena in Natural Sciences: Chaos, Fractals, Selforganization and Disorder: Concepts and Tools* (Springer-Verlag, Berlin, 2000).
[36] C. J. Pethick and H. Smith, *Bose-Einstein Condensation in Dilute Gases* (Cambridge University Press, Cambridge, U. K., 2002).